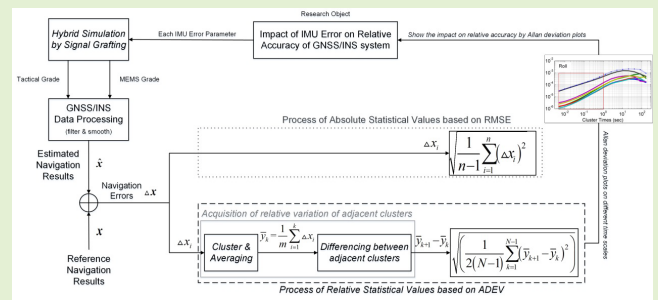


Impact Assessment of Various IMU Error Sources on the Relative Accuracy of the GNSS/INS Systems

Quan Zhang¹, Xiaoji Niu¹, and Chuang Shi

Abstract—GNSS/INS relative accuracy, which characterizes error variation or instability on different time/spatial scales, is increasingly required in some new applications, such as precise surveying and mapping, especially to represent the details of error variation over the short term for precise relative measurement. The INS, as an important GNSS/INS systems component, can provide high navigation accuracy over the short term, but INS navigation accuracy decreases with time due to IMU error sources, which might have a great influence on the GNSS/INS relative accuracy. This paper focuses on the impact assessment of IMU errors on GNSS/INS relative accuracy and proposes a hybrid simulation scheme based on signal grafting to analyze the impact of each IMU error on the relative accuracy. Allan variance, as one of the evaluation methods of GNSS/INS relative accuracy, is applied. The results show that the white noise of the gyroscope and accelerometer is the major factor affecting the GNSS/INS short-term accuracy, and the backward smoothing solution can further reduce the impact of nonwhite noise. This work can provide a reference for sensor selection and facilitate the use of low-end IMUs in applications with high demand for short-term relative accuracy.

Index Terms—GNSS/INS, relative accuracy, IMU error sources, time scales, Allan variance.



I. INTRODUCTION

THE integration of the global navigation satellite system (GNSS) and inertial navigation system (INS) can make the utmost of the high-precision long-term performance of GNSS and excellent short-term performance of INS and provide continuous and accurate navigation information; thus, GNSS/INS integration has been widely used in precision measurements, such as mobile mapping and precise track measuring [1], [2]. However, it has always been questionable

why the GNSS/INS systems of centimeter-level positioning can achieve millimeter precision measurement. In fact, this kind of precision measurement is essentially a temporal or spatial relative measurement, and it is more concerned with the relative variation of the navigation error on different time/spatial scales, not the overall error [3]–[5]. However, previous research has mainly focused on the centimeter-level absolute accuracy with dominant components of long-term error [6], [7]; only a few studies have focused on relative accuracy on different time/spatial scales [8], while research on the influencing factors of relative accuracy is relatively less.

Manuscript received December 25, 2019; revised January 8, 2020; accepted January 8, 2020. Date of publication January 13, 2020; date of current version April 3, 2020. This work was supported in part by the National Natural Science Foundation of China under Grant 41604020, in part by the General Financial Grant from the China Postdoctoral Science Foundation under Grant 2015M582275, and in part by the Special Financial Grant from the China Postdoctoral Science Foundation under Grant 2016T90729. The associate editor coordinating the review of this article and approving it for publication was Dr. Kagan Topalli. (Corresponding author: Xiaoji Niu.)

Quan Zhang and Xiaoji Niu are with the GNSS Research Center, Wuhan University, Wuhan 430079, China, and also with the Collaborative Innovation Center of Geospatial Technology, Wuhan University, Wuhan 430079, China (e-mail: zhangquan@whu.edu.cn; xjniu@whu.edu.cn).

Chuang Shi is with the School of Electronic and Information Engineering, Beihang University, Beijing 100083, China (e-mail: shichuang@buaa.edu.cn).

Digital Object Identifier 10.1109/JSEN.2020.2966379

The navigation accuracy of GNSS/INS integration is mainly affected by the GNSS positioning accuracy, inertial measurement unit (IMU) error sources, the optimal estimation algorithm and the vehicle dynamic. There has been some research on the effect of GNSS variance and vehicle manoeuvre [9], [10]. The suitable GNSS quality obtained by parameter tuning can guarantee effective and efficient prediction of states [11], and vehicle maneuvering is mainly related to the observability of parameter estimation in the Kalman filter [12]. The INS can maintain the navigation accuracy over the short term, but the accuracy decreases with time due to IMU errors, which might have great influence on the integrated navigation accuracy on a large time scale. Stand-alone

INS performance analysis was typically based on INS error dynamic equations to analyze the error propagation caused by IMU errors over the long term and short term [13], [14], but the key points considered only the INS drift error, and further analysis involving GNSS auxiliary information has not been conducted. Quantitative analysis of the impacts of IMU quality in GPS/INS deep integration based on the simplified error dynamics equations was carried out under stationary conditions and in specific high dynamic with continuous GPS updates [15], [16], but the focus of this work is mainly the maneuver-independent velocity error, which is essentially the drift error caused by IMU errors during the typical GNSS update interval (e.g., 1 s).

Some approaches for improving the relative accuracy of the GNSS/INS systems have briefly been given, and parameter tuning based on the Kalman filter by concretely enlarging the variance of the GNSS position update (measurement noise covariance matrix) was carried out to improve the relative accuracy [17]. The methods of adjusting the GNSS sampling rate and applying backward smoothing were proposed to improve the relative accuracy [18]. Gyro noise and residual drift error were briefly noted as an assistant indices for evaluating the relative accuracy of the position and orientation system (POS) [19]. However, there were no prior studies to assess the effect of IMU errors on GNSS/INS relative accuracy. The INS position drift error with a GNSS signal-interrupt was taken as the assessment indicator in the performance analysis of the GNSS/INS systems [20], and the inertial attitude determination performance on different time scales with the assistance of GPS was presented [21]. However, these indicators can describe only the statistics of the overall navigation error, and cannot describe the details of the error relative variation well enough.

A full analytical solution to the complete INS error dynamic equations is extremely complex, and it is difficult to analyze theoretically the IMU error propagation in the GNSS/INS solution considering the impact of GNSS assistance by optimal estimation, such as Kalman filter. On the one hand, it is feasible to simply solve the error dynamic equations and estimate the navigation system performance by taking into account simple vehicle maneuvers such as remaining stationary, and a combination of analysis and a simulation strategy is commonly applied to analyze the navigation accuracy of different grade systems [13]. On the other hand, the simulation is one common choice for navigation performance evaluation [14], [22]. The advantage of simulation method is mainly reflected in the following points: the vehicle dynamics and IMU data can be designed according to requirements [23], [24]; one can evaluate the impact of one certain factor [25]; and it can be implemented without any hardware cost. However, the existing simulation methods are either unable to generate the single error source or separated from field data. Therefore, a hybrid simulation scheme of signal grafting based on field datasets is proposed in this paper.

Currently, there is little research on how to analyze and improve the relative accuracy of the GNSS/INS systems considering the impact of IMU errors. This paper aims to analyze the impact of different IMU errors on the GNSS/INS relative

accuracy using the combination of simplified analysis and a simulation method to determine the major error. *It should be noted that the research on relative accuracy is carried out with continuous GNSS assistance to satisfy the high accuracy requirement of precision measurements.* This paper is organized in the following manner: section II gives the concept of relative accuracy and its evaluation method; the impact of IMU errors on GNSS/INS relative accuracy is given based on the simplified IMU error propagation and Kalman gain in section III; section IV describes the proposed simulation scheme; the data process solution and the discussion and analysis of the test results are given in section V; and section VI presents the conclusions.

II. GNSS/INS RELATIVE ACCURACY ON DIFFERENT TIME SCALES

The term “accuracy” generally denotes a statistical measure that provides the degree of conformance between the estimated or measured navigation parameters (e.g., position and/or velocity and/or attitude) of an object at a given time (or position) and the reference navigation parameters [26], [27]. Absolute accuracy with the dominance of systematic error quantifies the closeness of the navigation solution of the integrated system to the true navigation parameters, and it commonly involves a component of random error and a component of systematic error. It is usually expressed by the root mean square error (RMSE) as follows [28]:

$$\sigma_{rmse} = \sqrt{\frac{1}{n} \sum_{i=1}^n (\Delta x_i)^2} \quad (1)$$

where Δx_i represents the deviation between the measurements and reference true values, n is the sample number, and σ_{rmse} is the root mean square error. As evident from (1), the absolute accuracy can give only the overall degree of dispersion of the navigation error relative to the zero value, but it cannot show the relative variation between adjacent time intervals.

A. Concept of GNSS/INS Relative Accuracy

If the variable Δx_i in (1) is replaced with $\Delta x_i - \Delta \bar{x}$ ($\Delta \bar{x} = \frac{1}{n} \sum_{i=1}^n \Delta x_i$, it is the average of the sequence x_i , $i \in [1, n]$), then the calculation of the standard deviation (STD) can be written as [28]

$$\sigma_{std} = \sqrt{\frac{1}{n-1} \sum_{i=1}^n (\Delta x_i - \Delta \bar{x})^2} \quad (2)$$

The standard deviation is one of the common expressions of relative accuracy and it represents the degree of dispersion relative to the mean value. However, the relative variation is not limited to being relative to the mean; it can also refer to the relative relationship between the given epoch or clusters. Therefore, if the variable Δy_i is used to represent the relative variation of the navigation error in a given time scale τ , then the statistical deviation of the relative variation

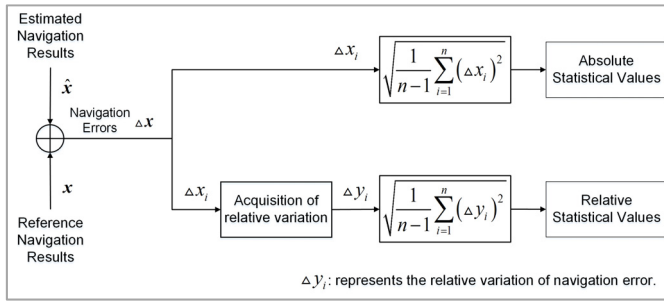


Fig. 1. Comparison between the absolute accuracy and relative accuracy concepts.

can be expressed as

$$\sigma(\tau) = \sqrt{\frac{1}{n-1} \sum_{i=1}^n (\Delta y_i)^2} \quad (3)$$

where Δy_i can, but is not limited to, be expressed in the following expression.

$$\Delta y_i = \begin{cases} \Delta x_m - \Delta x_n, & m \text{ and } n \text{ represents the different time} \\ & \text{or points;} \\ \frac{1}{n} \sum_{k=1}^n \Delta \bar{x}_k - \frac{1}{n} \sum_{k=n+1}^{2n} \Delta \bar{x}_k, & n \text{ represent the length of cluster;} \\ \text{other,} & \text{it represents the relative variation in a} \\ & \text{given scale.} \end{cases}$$

Here (3) is the common expression of relative accuracy based on the statistical deviation of the relative variation. Generally, the relative accuracy focuses on the relationship of the relative variation of the navigation error at a given time/spatial scale and is a statistical measure that provides the degree of relative variation regardless of any error in the true navigation solution. Relative accuracy, which mainly involves the component of random error, can reflect the characteristics of stability, correlation and smoothness of the navigation error.

Fig. 1 gives the different statistical forms, including the absolute and relative statistical values, which represent the total variation of the navigation error and the relative variation of the navigation errors, respectively. The absolute accuracy is achieved by analyzing the original navigation errors by the statistical method, which represents the difference between measured or estimated values \hat{x} and the reference or true values x . Hence, the study object of the absolute accuracy is the total variation of the navigation error itself. However, there is a different study object for the relative accuracy, which is to analyze the relative variation Δy_i of navigation error Δx_i . The acquisition of the relative variation depends on specific application requirements, and this paper presents an expression based on Allan variance in section II.B.

It is important and convenient to clearly define the absolute accuracy and the relative accuracy since in most cases the navigation error is composed of a slow varying signal with

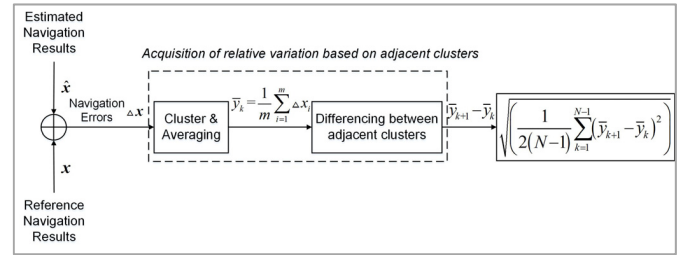


Fig. 2. Concept of relative accuracy in terms of Allan deviation.

almost no noise, while in some applications, it is the accuracy of the change in navigation that is most important (such as that in the precision mobile mapping) [2], [3].

B. Allan Variance

Allan variance (or the corresponding square root, the Allan deviation), as one of evaluation method of relative accuracy, is a method of representing the root mean square (RMS) random error as a function of the average time, which is widely used to characterize the instabilities of an oscillator or time series [29]–[31]. It can give an idea of how stable on average an oscillator or time series is over a given time scale. The formula of the Allan deviation (ADEV) can be expressed as follows [8]:

$$\sigma(\tau)_{allan} = \sqrt{\left(\frac{1}{2(N-1)} \sum_{k=1}^{N-1} (\bar{y}_{k+1} - \bar{y}_k)^2\right)} \quad (4)$$

where \bar{y} is the average of the sample data sequence y in a specific time interval τ , which is the time scale (from short term to long term); $\sigma(\tau)_{allan}$ is the corresponding Allan deviation shown in the Allan variance plot; and N is the total number of consecutive data points.

Fig.2 gives the representations of relative accuracy in terms of the Allan deviation. The “average sequence” is composed of the average of the navigation errors in the specified cluster that weaken or eliminate the high-frequency noise. The “difference sequence” represents the relative variation between adjacent clusters on different time scales, and it is applied as an input of the variance analysis to show the statistical values of the relative variation.

According to the length of the time cluster, GNSS/INS relative accuracy can be categorized into short-term accuracy (e.g., time scale is less than 1 s) and long-term accuracy (e.g., time scale is more than 10 s). There is an obvious difference between the short-term accuracy of the INS and the short-term relative accuracy of GNSS/INS integration. The former refers to the divergence of the stand-alone INS navigation error with time affected by IMU errors, while the latter represents the relative accuracy on a short time scale (namely, short-term stability or smoothness). However, there is a close relationship between them because the integrated navigation accuracy depends on the performance of the inertial sensors. Some research works related to the GNSS/INS relative accuracy on different time scales focused on using the Allan variance method to evaluate the short-term accuracy [8]. Hence, this paper will apply Allan variance to analyze different

impacts of the IMU errors on the relative accuracy of the GNSS/INS systems.

III. IMPACT ANALYSIS OF IMU ERROR SOURCES ON GNSS/INS RELATIVE ACCURACY

IMU errors are important factors of the INS drift error that influence the relative accuracy of GNSS/INS integration. The correction of navigation errors aided by GNSS assistance will be reduced if the INS drift error over a short time is small (i.e., the INS short-term accuracy is good), which can guarantee the stability or smoothness of the integrated navigation error and thus improve the short-term relative accuracy of the GNSS/INS systems. Therefore, the propagation of IMU errors based on the simplified INS error dynamic equations is briefly introduced first in this section. Then, the effect of IMU errors on GNSS/INS relative accuracy based on the Kalman gain is illustrated to show the major factors of GNSS/INS relative accuracy.

A. Propagation Analysis of IMU Errors through Simplified INS Error Dynamic Equations

The propagation of IMU errors in a given frame can be defined by the set of coupled differential equations based on inertial navigation equations. The phi-angle error dynamic equations with respect to the navigation reference frame can be written as follows [13], [32]:

$$\begin{aligned}\delta\dot{\mathbf{r}}^n &= \mathbf{F} \cdot \delta\mathbf{r}^n + \delta\mathbf{v}^n \\ \delta\dot{\mathbf{v}}^n &= \delta\mathbf{f}^n + \mathbf{f}^n \times \boldsymbol{\phi} - (\boldsymbol{\omega}_{ie}^n + \boldsymbol{\omega}_{in}^n) \times \delta\mathbf{v}^n \\ &\quad + \mathbf{v}^n \times (\delta\boldsymbol{\omega}_{ie}^n + \delta\boldsymbol{\omega}_{in}^n) + \delta\mathbf{g}^n \\ \dot{\boldsymbol{\phi}} &= -\boldsymbol{\omega}_{in}^n \times \boldsymbol{\phi} - \delta\boldsymbol{\omega}_{ib}^n + \delta\boldsymbol{\omega}_{in}^n\end{aligned}\quad (5)$$

where all parameters are with respect to the navigation frame. All symbols are defined as follows: \mathbf{F} is the coefficient matrix of the position error; $\delta\mathbf{r}^n$, $\delta\mathbf{v}^n$ and $\boldsymbol{\phi}$ represent the position, velocity and attitude error in the navigation frame respectively, with $\delta\dot{\mathbf{r}}^n$, $\delta\dot{\mathbf{v}}^n$ and $\dot{\boldsymbol{\phi}}$ being the corresponding time derivatives; $\boldsymbol{\omega}_{en}^n$, $\boldsymbol{\omega}_{ie}^n$ and $\boldsymbol{\omega}_{in}^n$ respectively represent the angular rate of the navigation frame relative to the earth frame, that of the earth frame relative to the inertial frame and that of the navigation frame relative to the inertial frame, respectively, with $\delta\boldsymbol{\omega}_{en}^n$, $\delta\boldsymbol{\omega}_{ie}^n$ and $\delta\boldsymbol{\omega}_{in}^n$ being the corresponding angular rate errors; \mathbf{f}^n is the specific force in the navigation frame; and $\delta\mathbf{g}^n$ is the normal gravity error in the local position. $\delta\mathbf{f}^n$ and $\delta\boldsymbol{\omega}_{in}^n$ represent the sensor errors of accelerometers and gyros, which mainly include the bias, scale factor and white noise. In this paper, vectors are denoted as bold lower case italic letters, matrices are denoted as bold upper case italic letters, and scalars are denoted as upper or lower case italic letters.

Here, the uncertainty of the sensors can be expressed as

$$\begin{aligned}\delta\mathbf{f} &= \mathbf{b}_f + \mathbf{S}_f \cdot \mathbf{f} + \boldsymbol{\varepsilon}_f \\ \delta\boldsymbol{\omega} &= \mathbf{b}_\omega + \mathbf{S}_\omega \cdot \boldsymbol{\omega} + \boldsymbol{\varepsilon}_\omega\end{aligned}\quad (6)$$

where \mathbf{b}_f and \mathbf{b}_ω are residual biases of the accelerometers and gyros respectively, \mathbf{S}_f and \mathbf{S}_ω represent the diagonal matrix (the corresponding vector forms are denoted as s_f and s_ω) of the residual scale factors of the accelerometers and

gyros respectively. $\boldsymbol{\varepsilon}_f$ and $\boldsymbol{\varepsilon}_\omega$ are the white noise of the accelerometers and gyros, respectively.

A complete analytical solution to the error dynamic equations is complicated, and it is extremely difficult to analyze the error propagation directly. Considering that the periods of independent INS navigation in GNSS/INS integration are only approximately several minutes or even seconds and that the errors caused by some terms such as the Coriolis, the gravity and the rotational angular rates are relatively small, and because the effect of IMU errors on navigation accuracy is the focus of this work, the error dynamic equations can be reduced to

$$\begin{aligned}\delta\dot{\mathbf{r}}^n &= \delta\mathbf{v}^n \\ \delta\dot{\mathbf{v}}^n &= \delta\mathbf{f}^n + \mathbf{f}^n \times \boldsymbol{\phi} \\ \dot{\boldsymbol{\phi}} &= -\delta\boldsymbol{\omega}_{ib}^n\end{aligned}\quad (7)$$

According to the simplified error dynamic equations, the angular error $\delta\theta(t)$ and position error $\delta r_\omega(t)$ related to time caused by the uncompensated gyro bias of a single direction (e.g., roll or pitch gyro) b_ω can be further reduced to the following form for a short time period [11]:

$$\delta\theta(t) = \int b_\omega dt = b_\omega \cdot t \quad (8)$$

$$\delta r_\omega(t) = \int v dt = \int \frac{1}{2} b_\omega \cdot g t^2 dt = \frac{1}{6} b_\omega \cdot g t^3 \quad (9)$$

where g is the gravitational acceleration and t is the duration of integration. Similarly, according to the simplified velocity and position error dynamic equations, the position error $\delta r_f(t)$ proportional to time caused by uncompensated accelerometer bias b_f can be expressed as [11]

$$\delta r_f = \int v dt = \int b_f \cdot t dt = \frac{1}{2} b_f \cdot t^2 \quad (10)$$

Unlike the error propagation of sensor biases, the simplified error dynamic equations cannot be applied to the random walk error growth, and it is a function of the standard deviation of the output noise, the sample frequency and the duration of integration [33]. The relationship between the standard deviation of angular error $\sigma_{\delta\theta}$ and that of gyro noise $\sigma_{\varepsilon_\omega}$ can be obtained by taking the expected results of the discrete simplified attitude error dynamic equation shown in (7) over a short time, and the standard deviation of the attitude error caused by the gyro noise is simplified as a function of time [34].

$$\sigma_{\delta\theta} = \sigma_{\varepsilon_\omega} \sqrt{T_s t} \quad (11)$$

where $T_s = 1/f_s$, with f_s being the sample frequency.

Similarly, the integration of accelerometer noise σ_{ε_f} and gyro noise $\sigma_{\varepsilon_\omega}$ produces the velocity error $\sigma_{\delta v}$ and the position error $\sigma_{\delta r}$, and the relationship between them can be obtained by taking the expected simplified velocity and position error dynamic equation shown in (7). Here, the stationary condition needs to be assumed, and the noise of the gyros and accelerometers are independent. Additionally, assuming that there is no correlation between the accelerometer bias and attitude error. In this case, inserting $\mathbf{f}^n \approx [0 \ 0 \ -g]^T$ into the simplified

TABLE I
SUMMARY OF IMPACT OF IMU ERROR ON
INS POSITION PERFORMANCE

Sensors	Error Sources	symbol	Power of Time	Coefficient of Effect on Position Drift Errors	
				North/East	Vertical
Gyro	bias	b_ω	t^3	$\frac{1}{6} \cdot g$	$\frac{1}{6} \cdot g$
	white noise	$\sigma_{\varepsilon_\omega}$	$t^{3/2}$	$gT_s \sqrt{\frac{T_s}{6}}$	0
Accel.	bias	b_f	t^2	$\frac{1}{2}$	$\frac{1}{2}$
	white noise	σ_{ε_f}	t	$\frac{\sqrt{2}}{2} T_s$	$\frac{\sqrt{2}}{2} T_s$

velocity error dynamic equation, the standard deviation of the velocity and position error (including the single horizontal and vertical direction) caused by the white noise of the gyroscope and accelerometer can be approximately expressed in the following forms (see Appendix):

$$\sigma_{\delta v_{horizontal}} = \sqrt{\sigma_{\varepsilon_f}^2 T_s t + \frac{1}{2} g^2 \sigma_{\varepsilon_\omega}^2 T_s^2 t^2}, \quad \sigma_{\delta v_{vertical}} = \sigma_{\varepsilon_f} \sqrt{T_s t} \quad (12)$$

$$\sigma_{\delta r_{horizontal}} = T_s t \sqrt{\frac{1}{2} \sigma_{\varepsilon_f}^2 + \frac{1}{6} g^2 \sigma_{\varepsilon_\omega}^2 T_s t}, \quad \sigma_{\delta r_{vertical}} = \frac{\sqrt{2}}{2} \sigma_{\varepsilon_f} T_s t \quad (13)$$

Since the scale factor is a maneuver -dependent error, we do not analyze its error propagation in this paper. Table I summarizes the growth of position error derived by different IMU errors based on the error propagation formulas (9), (10), (12) and (13). The position drift error caused by the bias, especially the gyro bias, diverges quickly with time. However, the impact of IMU errors on the short term accuracy or long term accuracy depends on the specific parameters configuration.

Here, a typical parameter configuration of MEMS IMU (the configuration is: data rate of 100Hz, gyro bias of $300^\circ/\text{h}$, gyro white noise of $3^\circ/\sqrt{\text{h}}$, accelerometer bias of 3000 mGal, and accelerometer white noise of $0.5\text{m/s}/\sqrt{\text{h}}$) is taken as an example to quantify the impact level of IMU error on position drift error. Fig.3 shows the INS horizontal position drift error in the given configuration.

It can be seen from Fig. 3 that IMU bias produces an obvious large short-term and long-term position error for the stand-alone INS navigation solution. Moreover, the gyro bias dominates the long-term position accuracy, while the accelerometer bias has a major impact on the short-term position accuracy as shown in the enlargement of Fig. 3. The white noise has limited impact on the long-term accuracy and short-term accuracy due to the high-frequency IMU data rate.

B. Impact Analysis of IMU Errors on GNSS/INS Relative Accuracy through Kalman Gain

The Kalman filter is a common optimal estimation method for integrating GNSS and INS measurements. Here, only

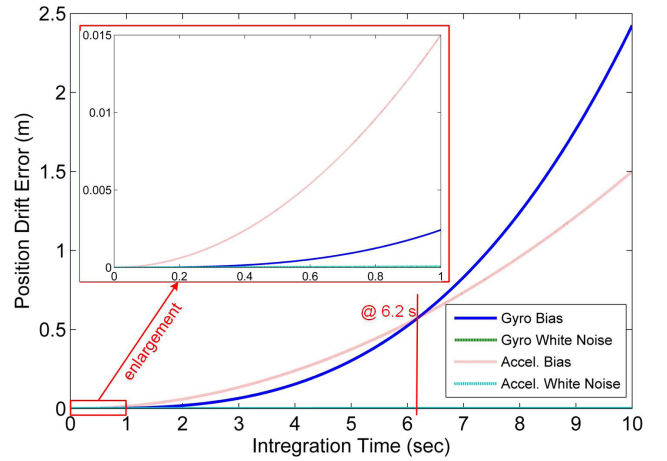


Fig. 3. The INS horizontal position drift error during the short term (< 1s) and long term (> 1s) in a given typical MEMS IMU configuration.

the prediction equation of the covariance matrix and the calculation of Kalman gain in a discrete form of the Kalman filter are presented to illustrate the effect of IMU errors on the navigation accuracy; more details on Kalman Filter are available in many articles [35]. This part mainly analyzes the impact of IMU errors on the GNSS/INS relative accuracy with continuous GNSS assistance when the filtering reaches a steady state. The prediction equation of the covariance matrix can be expressed as follows:

$$\mathbf{P}_{k/k-1} = \Phi_{k-1} \mathbf{P}_{k-1/k-1} \Phi_{k-1}^T + \mathbf{Q}_k \quad (14)$$

where $\mathbf{P}_{k/k-1}$ is the predicted estimate of the covariance matrix, Φ_{k-1} is the state transition matrix, \mathbf{Q}_k is the covariance matrix of system process noise, which is generally assumed to be white noise, and the $k-1$ represents the time, the T represents the transpose of a matrix.

It can be seen that the predicted covariance matrix $\mathbf{P}_{k/k-1}$ is related to the system noise covariance matrix \mathbf{Q}_k and the previous updated or predicted covariance matrix $\mathbf{P}_{k-1/k-1}$ that basically depends on the initial covariance matrix \mathbf{P}_0 and \mathbf{Q}_k . \mathbf{P}_0 mainly affects the initial convergence and has little influence on the state estimates if it is given a reasonable value. \mathbf{Q}_k is the main factor of $\mathbf{P}_{k/k-1}$ in addition to affecting the convergence characteristics of the state variables.

The Kalman gain \mathbf{K}_k is the relative weight provided for the measurement and the predicted state estimate. With a low gain, the filter places more weight on the predictions. In contrast, the filter follows the current measurements more closely. The equation of the Kalman gain in fraction form is

$$\mathbf{K}_k = \frac{\mathbf{P}_{k/k-1} \mathbf{H}_k^T}{\mathbf{H}_k \mathbf{P}_{k/k-1} \mathbf{H}_k^T + \mathbf{R}_k} \quad (15)$$

where \mathbf{H}_k is the measurement design matrix and \mathbf{R}_k is the covariance matrix of the measurement noise.

Because the predicted covariance matrix is strongly correlated with the system noise covariance matrix as shown in (14), substitute (14) into (15) to yield

$$\mathbf{K}_k = \frac{(\Phi_{k-1} \mathbf{P}_{k-1/k-1} \Phi_{k-1}^T + \mathbf{Q}_k) \mathbf{H}_k^T}{\mathbf{H}_k (\Phi_{k-1} \mathbf{P}_{k-1/k-1} \Phi_{k-1}^T + \mathbf{Q}_k) \mathbf{H}_k^T + \mathbf{R}_k} \quad (16)$$

TABLE II

IMPACT OF THE MATRIX OF SYSTEM NOISE ON RELATIVE ACCURACY

Tendency	Kalman gain K_k	Dependence of the current measurement	Smoothness of estimated results	Change of relative accuracy
$Q_k \rightarrow 0$	$K_k \rightarrow \frac{1}{H + \frac{R}{\Phi P \Phi^T H^T}}$	less	smooth	Good
$Q_k \rightarrow \infty$	$K_k \rightarrow \frac{1}{H}$	more	jumpy	Poor

It is clear that K_k is up to R_k and Q_k . Certainly, in this case, we assume that the measurement noise is reasonable and reliable; thus, Q_k , which defines how well the prediction can be trusted, is critical for achieving practical results by tuning the weight between the measurement and the predicted state estimate. As shown in Table II, the current measurement is trusted increasingly less as Q_k approaches zero, and the navigation correction aided by GNSS will be reduced to keep the estimated navigation results smooth, whereas the current measurement is trusted increasingly more as Q_k approaches infinity, and the navigation correction aided by GNSS will be enhanced to break the smoothness of the estimated navigation results. The smaller the IMU noise, the smaller the Q_k matrix, and the smaller the jumps by GNSS corrections. At the estimated navigation results, while a low gain close to zero will smooth out noise. The errors of the inertial sensors are defined by white noise within the system noise covariance matrix; thus, the IMU white noise will affect the smoothness of the estimated navigation results.

In addition, the IMU bias and scale can be estimated and compensated effectively by error modeling in the GNSS/INS integration when the Kalman filter reaches a steady state. There are only the residual bias and scale factor producing the navigation drift error over the short term (e.g. 1 s, before the next GNSS comes), and the corresponding navigation drift errors during one second are relatively small.

Here, we consider a simple example of a typical tactical-grade IMU. Assuming the white noise of gyros is $0.1^\circ/\sqrt{h}$ and the residual bias error of gyro is $0.5^\circ/h$, the corresponding attitude drift errors during one second are 0.0017° and 0.00014° , respectively, according to (11) and (8). The former is 10 times larger than the latter, which means that the IMU noises dominate the short-term errors of the navigation result. Moreover, the IMU white noise cannot be modeled and compensated, and it not only produces the drift INS navigation errors (perhaps this will not be obvious over a short time) but also has an effect on the smoothness of the estimated navigation results by reflecting the Q matrix of Kalman filter. Therefore, the IMU white noise will be the key factor of the GNSS/INS relative accuracy especially the short-term accuracy.

IV. HYBRID SIMULATION SCHEME

The proposed hybrid simulation scheme is a testing method that generates IMU data containing only one type of error source through signal grafting. The hybrid simulation method

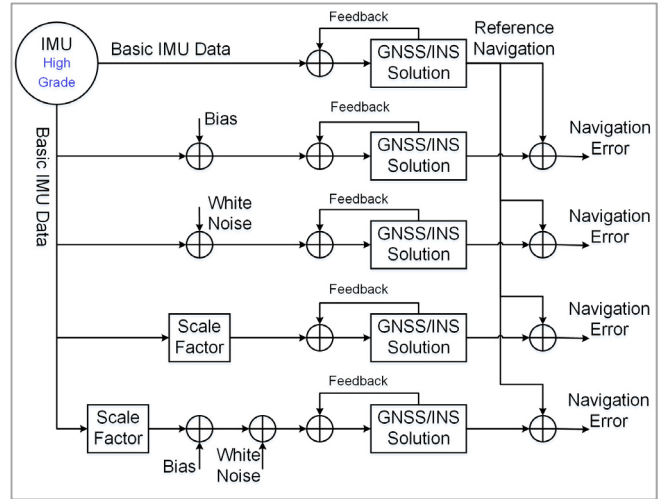


Fig. 4. Schematic diagram of the proposed hybrid simulation.

TABLE III

SPECIFICATIONS OF DIFFERENT-GRADE IMUS

Sensor	Error Sources	Ref. Sys.	Sim. Sys. #1	Sim. Sys. #2
		Navigation	Tactical	MEMS
Gyro	bias instability ($^\circ/h, 1\sigma$)	0.005	1	20
	scale factor (ppm, 1σ)	10	300	1000
	white noise ($^\circ/\sqrt{h}$)	0.0022	0.04	3
Accel.	bias instability (mGal, 1σ)	25	500	3000
	scale factor (ppm, 1σ)	10	300	1000
	white noise (m/s/ \sqrt{h})	0.001	0.05	0.5

takes the high-grade IMU data collected in the field test as basic data (i.e., true values of the IMU output), adds (or so-called grafts) each simulated IMU error (e.g., bias, scale factor, or noise) to the basic IMU data individually and processes the grafted IMU data using the GNSS/INS solution to obtain the different integrated navigation errors based on each IMU error. Fig. 4 shows the schematic diagram of the proposed hybrid simulation. It should be noted that the bias error and scale factor error can be modeled and augmented to the Kaman filter for on line estimation; thus, there is the feedback correction of IMU errors. However, the white noise cannot be estimated online due to the high-frequency variation.

This scheme of the proposed hybrid simulation can be described in detail as follows:

(a) Take real navigation-grade IMU measurements (their specifications are listed in Table III) as the basic data (i.e., true values of the IMU output), and regard its post-processed GNSS/INS solution as the “reference true values”.

(b) Simulate different types of IMU errors, including the bias, scale factor and white noise of gyros and accelerometers, and model the bias and scale factor as the 1st Gauss-Markov process.

$$\dot{\mathbf{y}} = -\frac{1}{\tau}\mathbf{y} + \boldsymbol{\omega} \quad (17)$$

where τ is the correlation time of a random process \mathbf{y} , and $\boldsymbol{\omega}$ is the corresponding driving white noise.

The specifications of different-grade IMUs (including tactical and micro-electro-mechanical system (MEMS)) can be found in Table III. Here, “Ref. Sys.” represents the reference system, as mentioned in (a), “Sim. Sys. #1” represents the simulated tactical-grade system, and “Sim. Sys. #2” represents the simulated MEMS-grade system.

(c) Add the simulated error to the basic data as expressed in (18); then, process these datasets in the mode of forward filtering and backward smoothing.

$$\begin{aligned} \mathbf{f}_1 &= \mathbf{f} + \mathbf{b}_f; & \mathbf{f}_2 &= (\mathbf{I} + \mathbf{S}_f) \cdot \mathbf{f}; & \mathbf{f}_3 &= \mathbf{f} + \boldsymbol{\varepsilon}_f \\ \boldsymbol{\omega}_1 &= \boldsymbol{\omega} + \mathbf{b}_\omega; & \boldsymbol{\omega}_2 &= (\mathbf{I} + \mathbf{S}_\omega) \cdot \boldsymbol{\omega}; & \boldsymbol{\omega}_3 &= \boldsymbol{\omega} + \boldsymbol{\varepsilon}_\omega \end{aligned} \quad (18)$$

where \mathbf{f} and $\boldsymbol{\omega}$ are the basic vectors of acceleration and angular rate, respectively; the numeral subscripts represent the simulated data with each IMU error in turn; \mathbf{I} represents the identity matrix.

(d) Add all simulated errors to the basic data, as expressed in (19), and then process the dataset in the mode of forward filtering and backward smoothing. The error parameters used in the data processing are consistent with those in the error simulation.

$$\begin{aligned} \mathbf{f}_{total} &= \mathbf{f} + \mathbf{b}_f + (\mathbf{I} + \mathbf{S}_f) \cdot \mathbf{f} + \boldsymbol{\varepsilon}_f \\ \boldsymbol{\omega}_{total} &= \boldsymbol{\omega} + \mathbf{b}_\omega + (\mathbf{I} + \mathbf{S}_\omega) \cdot \boldsymbol{\omega} + \boldsymbol{\varepsilon}_\omega \end{aligned} \quad (19)$$

where \mathbf{f}_{total} and $\boldsymbol{\omega}_{total}$ represent the simulated IMU data containing all IMU errors.

For the data acquisition in the field test, we cannot collect the output of gyros and accelerometers, which contains only one kind of IMU error. Here, the proposed hybrid simulation, similar to the adjoint simulation or signal grafting scheme, is utilized to determine the contribution of each IMU error to the GNSS/INS relative accuracy at a given time scale. Different variance analysis methods (especially Allan variance), as shown in Fig. 4, are applied to compare and analyze the impact of each IMU error on the GNSS/INS navigation accuracy, especially the short-term relative accuracy. This strategy can show the impact level of each IMU error on the relative accuracy by contributing to the increase in the values of the Allan deviation of the navigation errors. Next, a detailed description of the results and the discussion are given.

V. RESULTS AND DISCUSSION

To analyze the impact of each IMU error on the relative accuracy of the GNSS/INS system, a field test was conducted in the open sky by the Mobile Multi-Sensor System (MMSS) group at the University of Calgary to obtain the basic data used in the hybrid simulation scheme. The GNSS/INS system with a

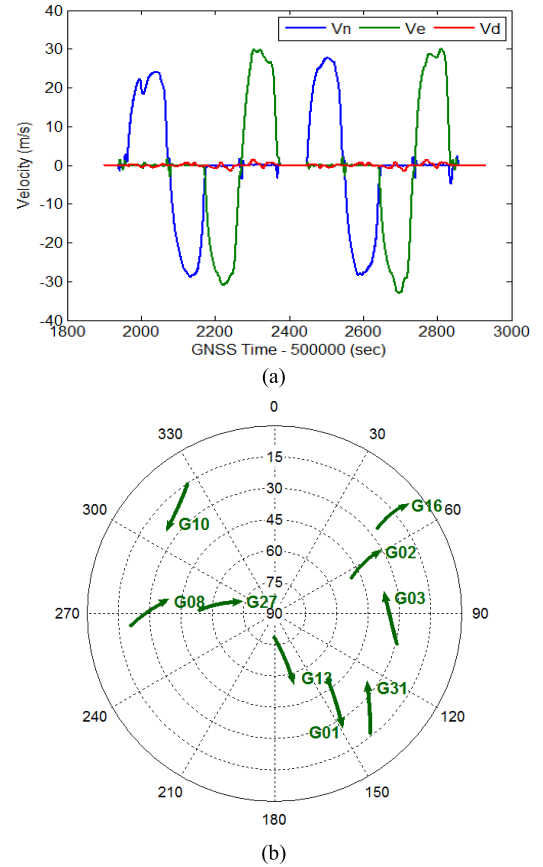


Fig. 5. Description of field test conditions: (a) vehicle velocity plot and (b) GPS satellite sky plot.

navigation-grade IMU was used as the reference system and to provide the basic IMU data, with a data rate of 200 Hz. A high-accuracy GNSS post-processed kinematic (PPK) solution with a GNSS data rate of 1 Hz and a dual frequency L1/L2 carrier phase was applied for the GNSS data processing to ensure high-precision GNSS positioning and reduce the effect of measurement noise on the GNSS/INS integrated navigation accuracy. Fig. 5 gives the velocity plots and GPS satellite sky plot used to describe the vehicle dynamics and the open-sky environment. There are many turns and U-turns to ensure enough dynamic, and the number of visible GPS satellites is approximately 9.

The GNSS/INS integration approach was applied to evaluate the impact of IMU errors on the relative accuracy because the signal quality of GNSS satellites in open-sky environment is relatively good. The system state model of the approach can be expressed as $\delta\mathbf{x} = [\delta\mathbf{r} \ \delta\mathbf{v} \ \boldsymbol{\phi} \ \mathbf{b}_\omega \ \mathbf{b}_f \ s_\omega \ s_f]^T$, which is given by navigation error states (including position error, velocity error and attitude error) and IMU error states (including the bias and scale factor of gyros and accelerometers) [36]. RTS backward smoothing, which is a well-known fixed-interval backward smoothing method in post-processed GNSS/INS solution to improve the estimated accuracy [37], [38], was applied to further analyze the effect of IMU errors on the relative accuracy of GNSS/INS. Fig. 6 gives the flow chart of GNSS/INS integrated data processing (that is the GNSS/INS solution shown in Fig. 4), and here the difference of the

TABLE IV
 STATISTICAL VALUES (RMSE) OF THE NAVIGATION ERROR BASED ON DIFFERENT
 IMU ERRORS OF THE TACTICAL GRADE USING FORWARD FILTERING

Error Source ¹	Position error (m)			Velocity error (m/s)			Attitude error (degree)		
	North	East	Down	North	East	Down	Roll	Pitch	Yaw
abias	0.0121	0.0113	0.0097	0.0027	0.0022	0.0016	0.0010	0.0012	0.0060
asf	0.0131	0.0136	0.0092	0.0017	0.0019	0.0013	0.0005	0.0007	0.0053
awn	0.0106	0.0107	0.0107	0.0021	0.0021	0.0019	0.0005	0.0008	0.0054
gbias	0.0133	0.0131	0.0132	0.0020	0.0020	0.0009	0.0008	0.0013	0.0112
gsf	0.0134	0.0128	0.0133	0.0019	0.0018	0.0009	0.0009	0.0009	0.0091
gwn	0.0107	0.0108	0.0129	0.0025	0.0024	0.0010	0.0023	0.0025	0.0122
all	0.0107	0.0101	0.0104	0.0037	0.0030	0.0024	0.0034	0.0049	0.0252

¹ From top to bottom in the table the IMU error types are, in order, accelerometer bias, accelerometer scale factor, accelerometer white noise, gyro bias, gyro scale factor, gyro white noise and all IMU errors.

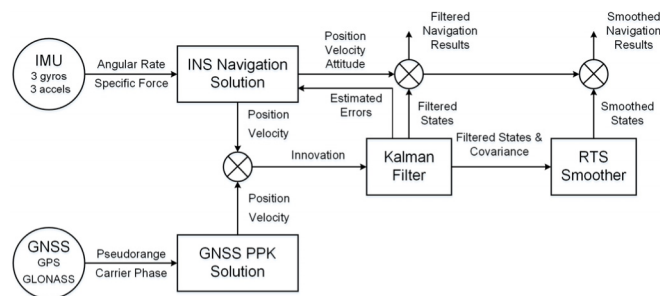


Fig. 6. Flow chart of GNSS and IMU data processing in the loosely-coupled mode.

position and velocity between INS navigation solution and GNSS PPK solution is the input to the Kalman filter.

A. Analysis of Tactical-Grade IMU in the Kalman Filter Mode

Table IV lists the traditional statistical values (e.g., RMSE) of the navigation errors based on different IMU errors of the tactical grade in the forward filtering mode. It can be seen that the position errors and velocity errors caused by different IMU errors are basically at the same level, and there is no significant difference between them; the roll and pitch errors caused by gyro white noise are more than 0.002°, which is more than 2 times that caused by other types of IMU errors; the gyro errors, especially bias and white noise, are the major contributors of the yaw error because there is approximately 2 times as much difference between the navigation results. The traditional statistics mainly reflect the overall variation of the navigation errors, and they cannot give the relative variation on different time scales.

Fig. 7 shows Allan variance plots of tactical-grade GNSS/INS navigation errors (including the three-dimensional position, velocity and attitude from top to bottom) with different types of IMU errors in the forward filtering mode. The horizontal axis represents the different time scales, and the vertical axis represents the Allan deviation of navigation errors

corresponding to each time scale. Here, “short-term” mainly refers to the range from 0.005 s to 1.0 s of the time scale, as marked in Fig. 7, while “long-term” mainly means that the time scale is more than 10 s. It is clear from Fig. 7 that the long-term error dominates the overall error because the Allan deviations of the long-term time scales are obviously larger than that of the short-term time scales, and the performance of the long-term error is basically consistent with the statistical values shown in Table IV.

To quantify the impact of each IMU errors on the short-term accuracy, the impact ratio can be defined as

$$ratio = \frac{1}{n} \sum_{i=1}^n \left(\frac{ADEV_{one}}{ADEV_{all}} \right)_i \quad (20)$$

where $ADEV_{one}$ represents the Allan deviation of navigation error based on the single IMU error, $ADEV_{all}$ represents the Allan deviation of navigation error based on all IMU errors, n is the total number of Allan deviation from 0.005 s to 1 s, i is the i -th epoch of the corresponding cluster time. Here the impact ratio is defined as the mean value of Allan deviation based on the single IMU error relative to that based on all IMU errors over the short term range, and it can show the overall impact level of IMU error on short-term relative accuracy. *The closer the ratio is to 1, the greater the impact of the corresponding IMU error on relative accuracy.*

Fig. 8 shows the ratio of the Allan deviations based on each IMU errors for tactical-grade GNSS/INS systems in the forward filtering mode. It can be seen that there is no obvious difference between the short-term horizontal position accuracy caused by different types of IMU errors because the difference in the ratios is not significant. Accelerometer errors, especially the white noise, are the main factor of the short-term vertical position accuracy.

For the short-term accuracy of velocity, the ratio based on accelerometer white noise is more than 0.8, which is approximately 5 times larger than those based on other types of IMU errors, a feature that is not shown in the traditional statistics listed in Table IV. Gyro errors have no prominent influence on the vertical velocity accuracy because the corresponding

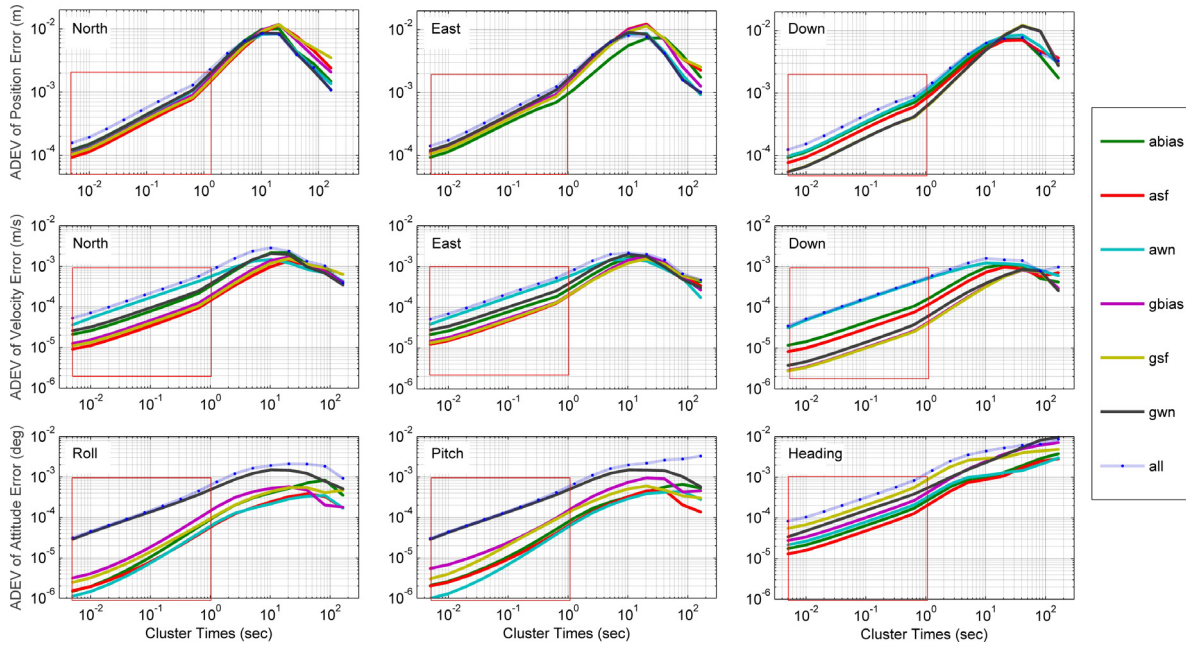


Fig. 7. Allan deviation (ADEV) plots of tactical-grade GNSS/INS navigation errors using forward filtering. From top to bottom on the figure, the plots are, in order, three-dimensional position, velocity and attitude; the marked range from 0.005 s to 1 s is the “short-term” being considered.

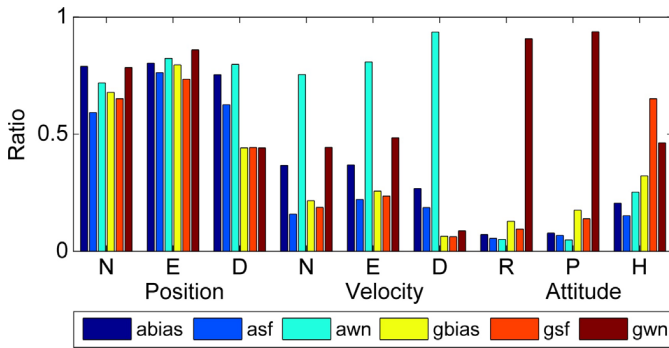


Fig. 8. The ratio of the Allan deviations based on each IMU errors for tactical-grade GNSS/INS systems in the forward filtering mode.

ratios are less than 0.1 and the coupling between the vertical velocity and gyro errors is weak.

For the short-term accuracy of horizontal attitude, the ratio based on gyro white noise is approximately 0.9, which is approximately 10 times larger than those based on other types of IMU errors. There is no significant difference in the ratio of the heading error corresponding to gyro errors, but the short-term yaw accuracy is obviously influenced by scale factor of gyros due to weak observability of gyro errors along the yaw direction, this is also a different performance from the statistical results representing the absolute accuracy with the dominance of long-term error.

B. Analysis of Tactical-Grade IMU in the Backward Smoothing Mode

Table V lists the traditional statistical values (e.g., RMSE) of the navigation errors based on different IMU errors of the tactical grade in the backward smoothing mode. Compared to Table IV, the backward smoothing improves the navigation

absolute accuracy because the estimated accuracy is improved by utilizing all the measurements. It can be seen that the white noise of gyros and accelerometers obviously affects the impact on the horizontal position and velocity errors; there is more than 2 times as much difference between the navigation results. The attitude errors caused by gyro white noise are more than 2 times larger than those caused by other types of IMU errors. Although backward smoothing can improve the estimation accuracy of the bias and scale factor that can be compensated in the GNSS/INS solution, it yields little reduction of the navigation errors caused by IMU white noise.

Fig. 9 shows Allan variance plots of tactical-grade GNSS/INS navigation errors with different types of IMU errors in the backward smoothing mode. Compared to Fig. 7, the impact of IMU white noise on the short-term accuracy is made obvious by utilizing the backward smoothing mode, which improved the estimation accuracy of the navigation errors and IMU bias and scale factor that are compensated well. From the values of the Allan deviation at the large time scale (e.g., more than 10 s), the long-term horizontal accuracy (including position, velocity and attitude) is significantly affected by the IMU white noise and accelerometer bias, while the long-term vertical position and velocity accuracy are affected by the accelerometer errors. The long-term yaw accuracy is significantly affected by the gyro errors, which is consistent with the statistical results shown in Table V

Fig. 10 shows the ratio results in the short term corresponding to Fig. 9. For the short-term accuracy of position, the accelerometer white noise is the main factor because the corresponding ratio is more than 0.9. The gyro white noise has some effect on the short-term accuracy of horizontal position because the corresponding ratio is more than 0.65. Gyro errors

TABLE V
 STATISTICAL VALUES (RMSE) OF THE NAVIGATION ERROR BASED ON DIFFERENT IMU ERRORS OF THE TACTICAL GRADE USING BACKWARD SMOOTHING

Error Source ¹	Position error (m)			Velocity error (m/s)			Attitude error (degree)		
	North	East	Down	North	East	Down	Roll	Pitch	Heading
abias	0.0058	0.0058	0.0064	0.0007	0.0008	0.0006	0.0006	0.0008	0.0013
asf	0.0011	0.0017	0.0061	0.0002	0.0002	0.0005	0.0002	0.0002	0.0004
awn	0.0071	0.0071	0.0064	0.0013	0.0013	0.0010	0.0005	0.0007	0.0016
gbias	0.0027	0.0020	0.0004	0.0003	0.0002	0.0001	0.0002	0.0003	0.0037
gsf	0.0006	0.0016	0.0006	0.0001	0.0002	0.0001	0.0003	0.0004	0.0054
gwn	0.0069	0.0068	0.0028	0.0010	0.0010	0.0002	0.0014	0.0022	0.0113
all	0.0075	0.0074	0.0069	0.0014	0.0014	0.0011	0.0024	0.0033	0.0206

¹ From top to bottom in the table the IMU errors type are, in order, accelerometer bias, accelerometer scale factor, accelerometer white noise, gyro bias, gyro scale factor, gyro white noise and all IMU errors.

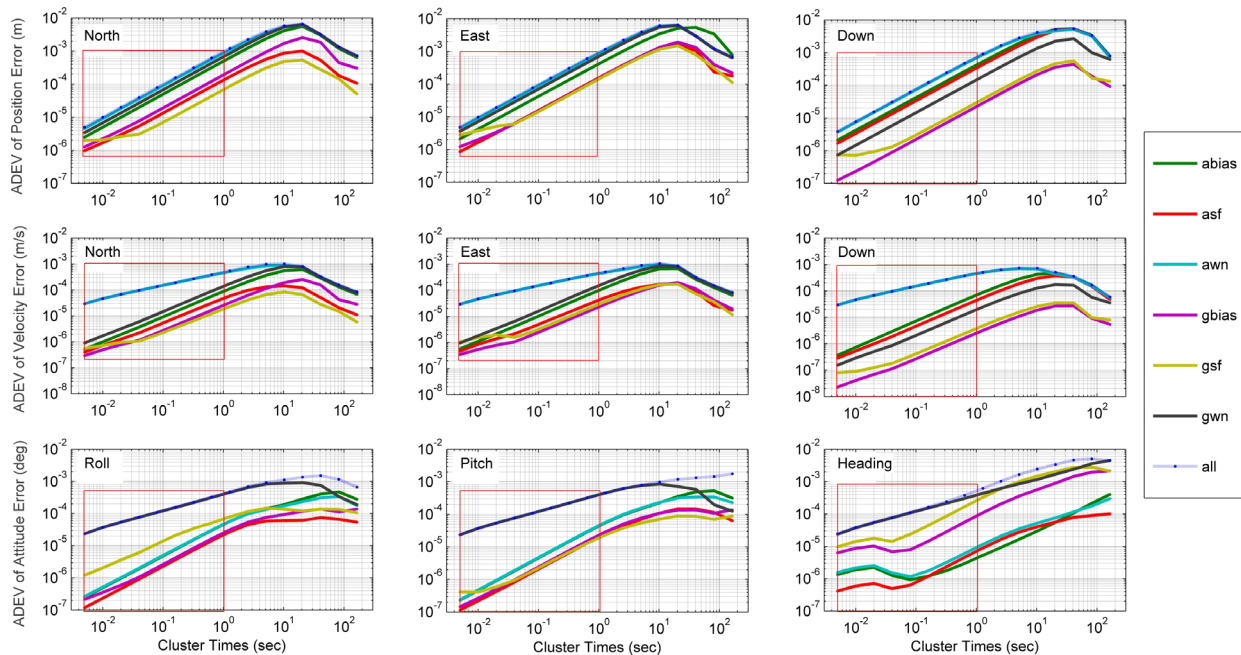


Fig. 9. Allan deviation (ADEV) plots of tactical-grade GNSS/INS navigation errors using backward smoothing. From top to bottom on the figure, the plots are, in order, three-dimensional position, velocity and attitude; the marked range from 0.005 s to 1 s is the “short-term” being considered.

have no prominent influence on the vertical position accuracy because the corresponding ratios are less than 0.2.

For the short-term accuracy of velocity, the ratio based on accelerometer white noise is approximately 1, which is more than 10 times larger than those based on other types of IMU errors. For the short-term accuracy of attitude, the gyro white noise becomes the major factor because the corresponding ratio is approximately 1, which is approximately 10 times larger than those based on other types of IMU errors.

The above analysis results of tactical-grade IMUs based on the traditional statistics and Allan variance show that the traditional statistics cannot show the relative accuracy on different time scales of the GNSS/INS systems, especially the short-term accuracy. IMU white noise is the major factor affecting the short-term accuracy of GNSS/INS systems, and

the backward smoothing solution can reduce the influence of the bias and scale factor which can be estimated and compensated by augmenting them as states in the integration solution. Next, considering that the short-term accuracy is the focus of this paper, we apply only the ratio plot of Allan deviation to further evaluate the impact of MEMS IMU errors on the short-term accuracy of the GNSS/INS systems to verify the consistency.

C. Analysis of MEMS IMU

Fig. 11 shows the ratio of the Allan deviations based on each IMU errors for MEMS-grade GNSS/INS systems in the forward filtering mode. For the short-term accuracy of position and velocity, the white noise and bias of accelerometer have a comparatively larger impact because the corresponding ratios

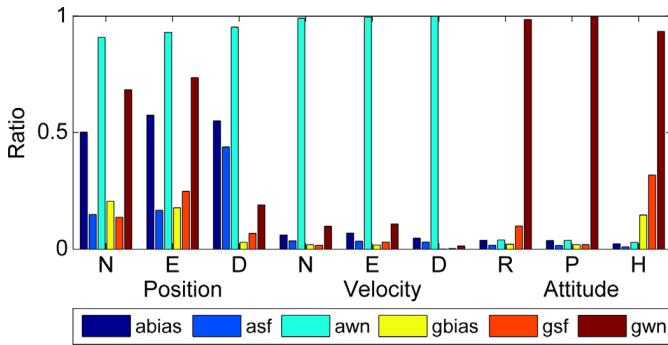


Fig. 10. The ratio of the Allan deviations based on each IMU errors for tactical-grade GNSS/INS systems in the backward smoothing mode.

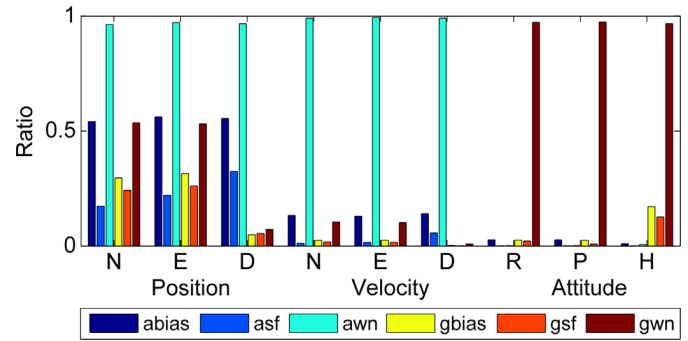


Fig. 12. The ratio of the Allan deviations based on each IMU errors for MEMS-grade GNSS/INS systems in the backward smoothing mode.

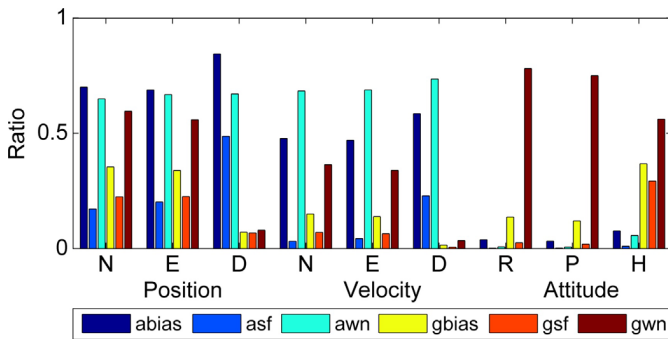


Fig. 11. The ratio of the Allan deviations based on each IMU errors for MEMS-grade GNSS/INS systems in the forward filtering mode.

are more than 0.7. The ratios based on gyro white noise are approximately 0.6 and 0.4, which indicates that gyro white noise yields a short-term position and velocity error. Gyro errors have almost no influence on the vertical component because of their weak coupling, and the corresponding ratios are less than 0.1.

For the short-term accuracy of horizontal attitude, the impact of the gyro white noise is relatively obvious, there is an approximately 10-fold ratio difference compared with other types of IMU errors. The gyro bias has a slight impact on the horizontal attitude. Gyro errors, especially the white noise, are the main factor of the short-term heading accuracy. Compared to the results of tactical-grade IMU shown in Fig. 8, although the white noise of gyro and accelerometer remains the dominant position, the impact of nonwhite noise, such as the bias, is prominent, as residual MEMS IMU errors still produce a large navigation drift error.

Fig. 12 shows the ratio of the Allan deviations based on each IMU errors for MEMS-grade GNSS/INS systems in the backward smoothing mode. It is clear that the accelerometer white noise has a relatively larger impact on the short-term accuracy of position and velocity, and there is a ratio that is close to 1 and is more than 2-fold difference compared with other types of IMU errors. The gyro white noise has certain degree influence on the horizontal component. The vertical component is mainly influenced by accelerometer errors. The gyro white noise is the major factor of the short-term attitude accuracy because the corresponding ratio is approximately 1, which is more than 10 times larger than that of other types

of IMU errors. Compared to Fig. 11, the backward smoothing solution reduces the impact of the bias and scale factor by improving their estimation accuracy in GNSS/INS solution to further highlight the impact of white noise on the short-term accuracy.

According to the analysis of tactical-grade and MEMS-grade IMUs, the white noise of gyros and accelerometers has a significant impact on the short-term accuracy of the GNSS/INS systems. The backward smoothing solution can reduce the impact of the bias and scale factor because they can be estimated better and compensated by error modeling in the GNSS/INS integration solution. For position and velocity, the absolute accuracy dominated by long-term errors mainly depends on the GNSS; thus, the change caused by different IMU errors is not obvious.

VI. CONCLUSIONS

A concrete expression of the relative accuracy was proposed to show the relative variation between adjacent clusters in a given time scale for precision measurements. The impact of the IMU error on the relative accuracy was analyzed through simplified INS error propagation and the Kalman gain to determine the difference and relation between the INS short-term accuracy and GNSS/INS relative accuracy. To analyze the performance of each IMU error, a hybrid simulation based on signal grafting was proposed to generate the IMU data dominated by one type of error.

Field test results show that the Allan deviations of the position error caused by different IMU errors are all less than 0.01 m in the short term scale, this can answer why the centimeter-level positioning systems can achieve the millimeter-level precision measurement. The IMU white noise is the key factor of the short-term accuracy because its ratio is more than 2 times larger than those based on other types of IMU errors, especially in the backward smoothing mode which can make the ratio of Allan deviations close to 1. The conclusions of this paper can provide guidance for accuracy improvement and promote the utilization of MEMS IMUs in applications with high demand for short-term relative accuracy. The next step is to find ways to enhance the attitude accuracy and reliability to reduce the impact of IMU errors on the long-term accuracy.

APPENDIX

- ① The differential form is $\delta \dot{\mathbf{v}}^n = \delta \mathbf{f}^n + \mathbf{f}^n \times \boldsymbol{\phi}$;
 ② The integration of the differential form results in

$$\delta \mathbf{v}^n = \int (\delta \mathbf{f}^n + \mathbf{f}^n \times \boldsymbol{\phi}) dt \quad (\text{A.1})$$

- ③ The discrete form is expressed as

$$\delta \mathbf{v}_k^n = \delta \mathbf{v}_{k-1}^n + (\delta \mathbf{f}^n + \mathbf{f}^n \times \boldsymbol{\phi}) T_s = \sum_{i=1}^k (\delta \mathbf{f}^n + \mathbf{f}^n \times \boldsymbol{\phi})_i T_s \quad (\text{A.2})$$

- ④ Here, the north velocity error is taken as an example, and $\mathbf{f}^n \approx [0 \ 0 \ -g]^T$. Take the expected value of both equation results in

$$\begin{aligned} & E \left[\delta v_{north}^n (\delta v_{north}^n)^T \right] \\ &= E \left[\left(\sum_{i=1}^k (\delta f_x^n + g \phi_y)_i T_s \right) \left(\sum_{i=1}^k (\delta f_x^n + g \phi_y)_i T_s \right)^T \right] \\ &= T_s^2 \sum_{i=1}^k E \left[(\delta f_x^n + g \phi_y)_i (\delta f_x^n + g \phi_y)_i^T \right] \end{aligned} \quad (\text{A.3})$$

- ⑤ There is no correlation between accelerometer bias and attitude error, that is, $E \left[\delta f^n (\phi_y)^T \right] = 0$. Here, $E \left[\delta f^n (\delta f^n)^T \right] = \sigma_{\varepsilon_f}^2$, $\sigma_{\delta\theta} = \sigma_{\varepsilon_\omega} \sqrt{T_s t}$ (Eq. (11)), $T_s k = t$ (T_s is the sampling interval, k is the number of discrete series, and t is the total integration time). Thus, the expected value of north velocity error is

$$\begin{aligned} \sigma_{\delta v_{north}}^2 &= T_s^2 \sum_{i=1}^k (\sigma_{\varepsilon_f}^2 + g^2 \sigma_{\varepsilon_\omega}^2 T_s^2 i) \\ &= T_s^2 \sigma_{\varepsilon_f}^2 k + T_s^4 g^2 \sigma_{\varepsilon_\omega}^2 \cdot \frac{1}{2} (k^2 + k) \end{aligned} \quad (\text{A.4})$$

That is,

$$\sigma_{\delta v_{north}} = \sqrt{\sigma_{\varepsilon_f}^2 T_s t + \frac{1}{2} g^2 \sigma_{\varepsilon_\omega}^2 T_s^2 (t^2 + T_s t)} \quad (\text{A.5})$$

The higher order term (i.e., 3^{rd} order) of T_s can be ignored because of the high data rate, and the above equations result in the following approximation

$$\sigma_{\delta v_{north}} = \sqrt{\sigma_{\varepsilon_f}^2 T_s t + \frac{1}{2} g^2 \sigma_{\varepsilon_\omega}^2 T_s^2 t^2} \quad (\text{A.6})$$

- ⑥ Here, $\mathbf{f}^n \approx [0 \ 0 \ -g]^T$, so there is no relationship between the vertical velocity error and gyro noise, and the expected value of vertical velocity error is

$$\sigma_{\delta v_{vertical}} = \sqrt{\sigma_{\varepsilon_f}^2 T_s t} = \sigma_{\varepsilon_f} \sqrt{T_s t} \quad (\text{A.7})$$

Similarly, the standard deviation of the position error (taking the north position error as an example) can be

deduced as follows:

$$\begin{aligned} & E \left[\delta r_{north}^n (\delta r_{north}^n)^T \right] \\ &= T_s^2 \sum_{i=1}^k E \left[\delta v_{north}^n (\delta v_{north}^n)^T \right] \\ &= T_s^2 \sum_{i=1}^k \sigma_{\delta v_{north}}^2 \\ &= T_s^2 \sum_{i=1}^k \left(\sigma_{\varepsilon_f}^2 T_s^2 i + \frac{1}{2} g^2 \sigma_{\varepsilon_\omega}^2 T_s^4 i^2 \right) \end{aligned} \quad (\text{A.8})$$

The expected value of north position error is

$$\sigma_{\delta r_{north}}^2 = T_s^4 \sigma_{\varepsilon_f}^2 \cdot \frac{1}{2} (k^2 + k) + \frac{1}{2} g^2 \sigma_{\varepsilon_\omega}^2 T_s^6 \left(\frac{1}{3} k^3 + \frac{1}{2} k^2 + c \frac{1}{6} k \right) \quad (\text{A.9})$$

The above equations result in the following approximation.

$$\sigma_{\delta r_{north}} = T_s t \sqrt{\frac{1}{2} \sigma_{\varepsilon_f}^2 + \frac{1}{6} g^2 \sigma_{\varepsilon_\omega}^2 T_s t} \quad (\text{A.10})$$

The standard deviation of the vertical position error is

$$\sigma_{\delta r_{vertical}} = \frac{\sqrt{2}}{2} \sigma_{\varepsilon_f} T_s t \quad (\text{A.11})$$

ACKNOWLEDGMENT

The authors would like to thank Dr N. El-Sheimy and the MMSS group at the University of Calgary for sharing the field test datasets that were used in this articles.

REFERENCES

- [1] Q. Chen *et al.*, "A railway track geometry measuring trolley system based on aided INS," *Sensors*, vol. 18, no. 2, p. 538, Feb. 2018.
- [2] K. Chiang, G. Tsai, H. Chang, C. Joly, and N. El-Sheimy, "Seamless navigation and mapping using an INS/GNSS/grid-based SLAM semi-tightly coupled integration scheme," *Inf. Fusion*, vol. 50, pp. 181–196, Oct. 2019.
- [3] Q. Chen, X. Niu, Q. Zhang, and Y. Cheng, "Railway track irregularity measuring by GNSS/INS integration," *J. Inst. Navigat.*, vol. 62, no. 1, pp. 83–93, Mar. 2015.
- [4] F. Zhu, W. Zhou, Y. Zhang, R. Duan, X. Lv, and X. Zhang, "Attitude variometric approach using DGNSS/INS integration to detect deformation in railway track irregularity measuring," *J. Geodesy*, vol. 93, no. 9, pp. 1571–1587, Sep. 2019.
- [5] A. Habib, K. I. Bang, A. P. Kersting, and D.-C. Lee, "Error budget of LiDAR systems and quality control of the derived data," *Photogramm. Eng. Remote Sens.*, vol. 75, no. 9, pp. 1093–1108, Sep. 2009.
- [6] M. Maaref and Z. M. Kassas, "A closed-loop map-matching approach for ground vehicle navigation in GNSS-denied environments using signals of opportunity," *IEEE Trans. Intell. Transp. Syst.*, to be published.
- [7] D. Bhatt, P. Aggarwal, V. Devabhaktuni, and P. Bhattacharya, "A novel hybrid fusion algorithm to bridge the period of GPS outages using low-cost INS," *Expert Syst. Appl.*, vol. 41, no. 5, pp. 2166–2173, Apr. 2014.
- [8] Q. Zhang, X. Niu, Q. Chen, H. Zhang, and C. Shi, "Using Allan variance to evaluate the relative accuracy on different time scales of GNSS/INS systems," *Meas. Sci. Technol.*, vol. 24, no. 8, Aug. 2013, Art. no. 085006.
- [9] K. Leung, J. Whidborne, D. Purdy, A. Dunoyer, and R. Williams, "A study on the effect of GPS accuracy on a GPS/INS Kalman filter," in *Proc. UKACC Int. Conf. Control*, Manchester, U.K., 2008.
- [10] U. Ojha, M.-Y. Chow, T. Chang, and J. Daniel, "Analysis on the Kalman filter performance in GPS/INS integration at different noise levels, sampling periods and curvatures," in *Proc. 35th Annu. Conf. IEEE Ind. Electron.*, 2009, pp. 2975–2980.

- [11] C. Goodall, X. Niu, and N. El-Sheimy, "Intelligent tuning of a Kalman filter for INS/GPS navigation applications," in *Proc. ION GNSS 20th Int. Tech. Meeting Satell. Division*, Fort Worth, TX, USA, 2007, pp. 2121–2128.
- [12] A. Borko, I. Klein, and G. Even-Tzur, "GNSS/INS fusion with virtual lever-arm measurements," *Sensors*, vol. 18, no. 7, p. 2228, Jul. 2018.
- [13] P. Savage, *Strapdown Analytics*, 2nd ed. Maple Plain, MN, USA: Strapdown Associates, 2007.
- [14] D. H. Titterton and J. L. Weston, *Strapdown Inertial Navigation Technology*, no. 7. London, U.K.: The Institution of Electrical Engineers, 2004, pp. 33–34.
- [15] Y. Ban, X. Niu, T. Zhang, Q. Zhang, and J. Liu, "Modeling and quantitative analysis of GNSS/INS deep integration tracking loops in high dynamics," *Micromachines*, vol. 8, no. 9, p. 272, Sep. 2017.
- [16] X. Niu, Y. Ban, Q. Zhang, T. Zhang, H. Zhang, and J. Liu, "Quantitative analysis to the impacts of IMU quality in GPS/INS deep integration," *Micromachines*, vol. 6, no. 8, pp. 1082–1099, Aug. 2015.
- [17] Q. Zhang, X. Niu, C. Liu, H. Zhang, C. Shi, and J. Zhao, "Approaches to evaluate and improve short-term relative accuracy of GPS/INS systems," in *Proc. IEEE/ION Position, Location Navigat. Symp.*, Apr. 2012, pp. 396–407.
- [18] Q. Zhang, X. Niu, and C. Shi, "Assessment of the effect of GNSS sampling rate on GNSS/INS relative accuracy on different time scales for precision measurements," *Measurement*, vol. 145, pp. 583–593, Oct. 2019.
- [19] *Applanix POS AV Specifications*. Accessed: Mar. 1, 2019. [Online]. Available: <http://www.applanix.com/media/downloads/products/specs/posav.pdf>
- [20] X. Niu, H. Zhang, C. Shi, and K. Chiang, "A proposed evaluation standard for the navigation results of MEMS INS/GPS integrated systems," presented at the Int. Symp. GPS/GNSS, 2010.
- [21] J. Skaloud, "Direct georeferencing in aerial photogrammetric mapping," *Photogramm. Eng. Remote Sens.*, vol. 68, no. 3, pp. 207–210, 2002.
- [22] X. Niu, Q. Wang, Y. Li, Q. Zhang, and P. Jiang, "An IMU evaluation method using a signal grafting scheme," *Sensors*, vol. 16, no. 6, p. 854, Jun. 2016.
- [23] C.-Q. Cheng, X. Cheng, X.-Y. Hao, and M.-D. Zhao, "Design and implementation of interactive strap-down inertial navigation simulation system for UAV," in *Proc. Sel. Papers Photoelectron. Technol. Committee Conf. Held*, Jan. 2016.
- [24] L. Aili, W. Huali, and D. Hongde, "Modeling and simulation of the warship deformation estimation based on inertial sensors," in *Proc. IEEE Chin. Guid., Navigat. Control Conf.*, Aug. 2014.
- [25] F. J. Zampella, A. R. Jimenez, F. Seco, J. C. Prieto, and J. I. Guevara, "Simulation of foot-mounted IMU signals for the evaluation of PDR algorithms," in *Proc. Int. Conf. Indoor Positioning Indoor Navigat.*, Sep. 2011.
- [26] B. Hofmann-Wellenhof, H. Lichtenegger, and E. Wasle, *GNSS—Global Navigation Satellite Systems: GPS, GLONASS, Galileo, and More*. Vienna, Austria: Springer, 2007.
- [27] *Accuracy (Trueness and Precision) of Measurement Methods and Results-Part 2: Basic Method for the Determination of Repeatability and Reproducibility of a Standard Measurement Method*, International Organization for Standardization, London, U.K., 1994.
- [28] R. Deakin and D. Kildea, "A note on standard deviation and RMS," *Austral. Surveyor*, vol. 44, no. 1, pp. 74–79, Jun. 1999.
- [29] D. Allan, "Time and frequency (time-domain) characterization, estimation, and prediction of precision clocks and oscillators," *IEEE Trans. Ultrason., Ferroelectr., Freq. Control*, vol. UFFC-34, no. 6, pp. 647–654, Nov. 1987.
- [30] Z. Malkin, "Application of the allan variance to time series analysis in astrometry and geodesy: A review," *IEEE Trans. Ultrason., Ferroelectr., Freq. Control*, vol. 63, no. 4, pp. 582–589, Apr. 2016.
- [31] J. Jurado, C. M. S. Kabbani, and J. Raquet, "A regression-based methodology to improve estimation of inertial sensor errors using Allan variance data," *Navigation*, vol. 66, no. 1, pp. 251–263, Jan. 2019.
- [32] E. H. Shin, "Estimation techniques for low-cost inertial navigation," Ph.D. dissertation, Dept. Geomatics Eng., Univ. Calgary Canada, Calgary, AB, Canada, 2005.
- [33] D. Gebre-Egziabher, "Design and performance analysis of a low-cost aided dead reckoning navigator," Ph.D. dissertation, Dept. Aeronaut. Astronaut., Stanford Univ., Stanford, CA, USA, 2004.
- [34] D. M. Bevely, A. Rekow, and B. Parkinson, "Evaluation of a blended dead reckoning and carrier phase differential GPS System for control of an off-road vehicle," in *Proc. 12th Int. Tech. Meeting Satell. Division Inst. Navigat.*, 1999, pp. 2061–2070.
- [35] Y. Liu, S. Li, Q. Fu, Z. Liu, and Q. Zhou, "Analysis of Kalman filter innovation-based GNSS spoofing detection method for INS/GNSS integrated navigation system," *IEEE Sensors J.*, vol. 19, no. 13, pp. 5167–5178, Jul. 2019.
- [36] X. Niu *et al.*, "Development and evaluation of GNSS/INS data processing software for position and orientation systems," *Survey Rev.*, vol. 47, no. 341, pp. 87–98, Mar. 2015.
- [37] K. Kim, J. Choi, J. Chung, G. Koo, I.-H. Bae, and H. Sohn, "Structural displacement estimation through multi-rate fusion of accelerometer and RTK-GPS displacement and velocity measurements," *Measurement*, vol. 130, pp. 223–235, Dec. 2018.
- [38] S. Nassar, X. Niu, and N. El-Sheimy, "Land-vehicle INS/GPS accurate positioning during GPS signal blockage periods," *J. Surveying Eng.*, vol. 133, no. 3, pp. 134–143, Aug. 2007.



Quan Zhang received the B.S. degree in geomatics engineering from the Shandong University of Science and Technology, in 2009, and the Ph.D. degree from Wuhan University, in 2015. From 2017 to 2018, he was a Postdoctoral Researcher with the Digital Photogrammetry Research Group (DPRG), Lyles School of Civil Engineering, Purdue University. He is currently a Research Assistant and a Postdoctoral with the GNSS Research Center and Collaborative Innovation Center of Geospatial Technology, Wuhan University. His research interests focus on inertial navigation and GNSS/INS integration technology.



Xiaoji Niu received the B.Eng. degree (Hons.) in mechanical and electrical engineering and the Ph.D. degree from Tsinghua University, Beijing, China, in 1997 and 2002, respectively. From 2003 to 2007, he was a Postdoctoral Fellow with the Mobile Multi-Sensor Systems (MMSS) Research Group, Department of Geomatics Engineering, University of Calgary. From 2007 to 2009, he was a Senior Scientist with SiRF Technology, Inc. He is currently a Professor with the GNSS Research Center, Wuhan University. His research interests focus on INS and GNSS/INS integration.



Chuang Shi received the B.Eng. degree in geodesy and the Ph.D. degree from Wuhan University, Wuhan, China, in 1991 and 1998, respectively. He has worked as an Expert in the field of earth observation and navigation for the 863 Program, the Leader of the expert panel of the navigation and location-based service project of the 12th Five-Year Plan, and the Deputy Chief Designer of the National Beidou Ground-Based Augmentation System. He is currently a Professor and a Ph.D. Supervisor of the School of Electronic and Information Engineering, Beihang University. He is also a Distinguished Professor of the Chang Jiang Scholars Program. He was a recipient of the National Science Fund for Distinguished Young Scholars.